Available online at www.sciencedirect.com
SCIENCE DIRECT
International Journal of Heat and Mass Transfer 49 (2006) 3914–3928
International Journal of HEAT and MASS TRANSFER
www.elsevier.com/locate/ijhmt

Computational prediction of a slightly heated turbulent rectangular jet discharged into a narrow channel crossflow using two different turbulence models

Manabendra Pathak, Anupam Dewan *, Anoop K. Dass

Department of Mechanical Engineering, Indian Institute of Technology Guwahati, Guwahati 781039, India

Available online 21 June 2006

Abstract

A computational investigation of three-dimensional mean flow field resulting due to the interaction of a rectangular heated jet issuing into a narrow channel crossflow has been reported in the present paper. The jet discharge slot spans more than 55% of the crossflow channel bed, leaving a small clearance between the jet edge and sidewalls. Such flow configurations are encountered in several industrial processes such as mixing product streams, drying product streams, etc. The objective of the present work was to carry out a detailed investigation of the mean flow field and flow structure, which could not be obtained in a similar two-dimensional experimental work reported in the literature. The commercial code FLUENT 6.2.16 based on the finite volume method was used to predict the mean flow and temperature fields for the jet to crossflow velocity ratio (R) = 6. Two different turbulence models, namely, Reynolds-stress transport model (RSTM) and the standard k–ε model, were used for the computations. Different terms of the Reynolds-stress transport equation were modeled based on the proposals in the literature that are appropriate for the important flow features of the present configuration. Important flow features predicted by the two models, such as the formation of different vortical structures and their effects on the flow field are discussed. Some predicted results are compared with the available experimental data reported in the literature. The predicted mean and turbulent flow properties are shown to be in good agreement with the experimental data. However, the performance of RSTM is found to be better than that of the standard k–ε model.

Keywords: Heated jet; Crossflow; Reynolds-stress transport model; Vortices; Turbulent mixing

1. Introduction

The flow fields of jets in a crossflow are encountered in several engineering and environmental applications, for example, in cooling tower, smoke issuing from smoke-stacks, chimneys, volcanoes, thermal discharges into river, film cooling of turbine blades, fuel injection for burners, V/STOL aircraft design, enhancement of industrial mixing and drying processes, etc. Because of its enormous applications and complex fluid flow phenomenon involved, the problem has been studied extensively by several researchers both experimentally and computationally during the last 50 years. There are several review papers on this topic including those by Margason [1], Holdeman [2], Sherif and Pletcher [3] and Acharya et al. [4]. The following three conclusions can be drawn from the literature review: (i) Most earliest studies of jet in crossflow were concerning the gross flow behaviour, such as, jet trajectory, jet penetration, jet spreading, etc. (ii) With the advancement of technology in both experimental and numerical fields, several new features of the flow field were analyzed in the literature such as the effects of velocity or momentum ratio, jet injection angle, skew angle, multiple jets, jet spacing, jet geometry, jet Reynolds number, impingements and swirl, etc. These studies extended the analysis of the flow field from the basic flow properties to the formation of different vortices,

* Corresponding author. Tel.: +91 361 2582656; fax: +91 361 2690762.
E-mail address: adewan@iitg.ernet.in (A. Dewan).

0017-9310/$ - see front matter © 2006 Elsevier Ltd. All rights reserved.
doi:10.1016/j.ijheatmasstransfer.2006.05.001

Nomenclature

C	model constant
c	model constant
D	width of the jet
g	acceleration due to gravity
k	turbulent kinetic energy
n	coordinate perpendicular to jet trajectory
P	mean pressure
Pr	Prandtl number
R	jet to crossflow velocity ratio (V_j/U_a)
R_{bj}	exit Richardson number
s	distance along the jet trajectory from the center of the jet slot
T	mean temperature
T_j	temperature of the jet
U	mean velocity along the crossflow direction (along the x direction)
U_a	crossflow velocity
U_s	component of mean velocity along s direction
V	mean velocity along the jet discharge direction (y direction)
V_j	jet velocity
V_n	component of mean velocity along n direction
W	mean velocity along spanwise (z direction)
x	coordinate along the crossflow direction
y	coordinate along the direction of jet discharge
z	coordinate along spanwise
δ	Kronecker delta
ε	rate of dissipation of turbulent kinetic energy k
μ	molecular viscosity
μ_t	eddy viscosity
ρ	density
σ_ε	model constant
σ_k	model constant
σ_t	turbulent Prandtl number
ϕ	model constant

Subscripts

a	crossflow condition
i, j, k	tensor notation
j	jet condition at the discharge

turbulent mixing and concentration studies. (iii) Though a variety of different geometries have been studied during the past few decades, a relatively few studies on the rectangular jet in crossflow have been reported in the literature and even fewer on the jet in a narrow crossflow channel have been reported. We intend to fill this lacuna through the present paper.

When a jet is discharged vertically into a crossflowing stream, the whole flow field can be classified in three distinct regions [5–7]. In the first region, the initially uniform jet flow interacts with the ambient crossflow causing a shear layer to develop at the jet boundaries. Upstream of this region, the crossflow is decelerated and a positive pressure region is formed. The length of the initial region depends on the jet diameter, velocity ratio and jet discharge Reynolds number. The second region is the main region or the established flow region, where the jet experiences maximum deflection. This region is complex, being characterized by the development of turbulent mixing layer around the jet boundaries and the flow becomes fully turbulent. Due to shearing action of the crossflow, the jet sides experience strong lateral deflections. The third region is the far-field region, where the jet axis approaches the crossflow direction asymptotically and the flow field becomes nearly self-similar. In this region, the magnitude and direction of the jet velocity are close to those of the crossflowing stream and it becomes difficult to distinguish between crossflow and jet fluids. The whole flow field of a jet in crossflow is characterized by four main vortical structures: (i) shear layer vortices; (ii) horseshoe vortices; (iii) wake vortices; and (iv) counter-rotating vortices [8,9]. As stated earlier, the shear layer vortices form near the initial region of the jet due to the interaction of the uniform jet velocity and the crossflow. These shear layer vortices form on the leeward and windward edges of the jet and have been attributed to Kelvin–Helmholtz type instabilities [9,10]. Due to the adverse pressure gradient upstream of the jet, a horseshoe vortex system is formed which wraps around the base of the jet and travels downstream. The wake vortices form in the second region and at the inner part of the jet. Experimental studies [8–10] and computational studies [11,12] support the fact that wake vortices are initiated by the entrainment of the crossflow boundary-layer into the wake and the upward re-orientation of the entrained flow into the wake structures. Lim et al. [13] observed that the size of the wake region depends upon the velocity ratio (R). For high velocity ratios ($R > 2$), the jet penetrates significantly into the crossflow and it bends over far enough downstream of the injection hole. Therefore, for these types of jets, there is little influence of the wall on its development. Moreover, there is a little effect of crossflow boundary layer characteristics on the flow for high values of R as the jet is able to penetrate through a relatively thin boundary layer. On the other hand for low velocity ratios, i.e., $R < 1$, the jet bends over into the wall at a small downstream distance and then it spreads over the wall. There is a lack of the wake region downstream of the jet injection hole and the jet behaves like a wall jet. In this type of situation, the jet flow is unable to cross the crossflow boundary layer and thus producing less complex flow behaviour in the near field of the jet compared to that with a high value of R. The counter-rotating vortices (CRVP) form at the

vertical plane just after the jet hole and these become dominant structures downstream in the flow field. These are formed due to both the shearing between the jet and the crossflow and the vorticity issuing from the jet hole exit [10]. However, there are different mechanisms proposed in the literature on the re-orientation of the jet hole vorticity into the CRVP structures. Peterson and Plesniak [14,15] have studied the development of these structures from the inlet plenum through the injection hole and out into the crossflow using PIV. Sau et al. [12] have also explicitly described the formation of CRVP and its growth. Besides these four structures, some authors [9,15–18] have reported the presence of secondary structures in the flow field. They have found an additional pairs of counter rotating vortices located between the jet and wall, thus bifurcating the traditional CRVP.

The flow structures that have been discussed in the above-mentioned studies are mostly for a round jet in crossflow. Several researchers have found that the structure of the flow field of square jets in crossflow is nearly identical to the flow field of round jet in crossflow. Liscinsky et al. [19] observed the similarity of flow field between the square jet and round jet in crossflow in terms of the mixing effectiveness. The different vortical structures, present in the flow field of round jet in crossflow are also reported in the flow field of square jet in crossflow [12,20–23]. A square jet can be treated as a special type of rectangular jet with discharge hole aspect ratio one. Welson and Thames [24] compared the pressure field around rectangular and circular jets. They found that a streamwise-oriented slot generates a pressure profile similar to a round jet. Humber et al. [25] experimentally studied a rectangular jet in crossflow and found similar observations of the jet penetration and trajectory as those in round jet in crossflow but observed more entrainment than that in the round jet case. Vincenti et al. [26] studied planer jets in crossflow at low Reynolds number using PIV. They studied the effect of velocity ratio on the interaction between the shear layer vortices and the counter rotating vortices. They observed that for the velocity ratios $R = 3$–6, the shear layer of the planer jet has large fluctuations and its instability seems to be driven by the action of the crossflow leading to the formation of wake like vortices. For velocity ratio higher than 6 they observed two types of shear layer vortices. Recently, Plesniak and Cusano [27] studied the confined rectangular jet in crossflow. They observed that the flow is more complex than a canonical unconfined round jet in crossflow. They also observed that the large-scale CRVP structures dominate the scalar mixing of both the jet and crossflow. Therefore, it may be concluded that most previous studies on jet in crossflow deal with round jet. However, the mechanism of formation and the governing flow physics for the square or rectangular jets in crossflow reveal some similarities to that for the case of round jet in crossflow, even though there may appear small quantitative differences in the local flow properties for the two cases.

In most practical situations, jets and plumes are either discharged vertically or at an angle to a crossflow. In such flow conditions, the jet and crossflow interaction and thermal spread are extremely important factors. Accordingly, when the temperature field is strongly affected by the velocity field and can be regarded as a passive scalar, it is necessary to understand the mean and statistical characteristics of the thermal spread and mixing in such jets in crossflow. The flow behaviour and heat transfer analysis of a heated jet in crossflow are reported by several researchers [28,29,6,30–34]. Chen and Hwang [29] experimentally studied a two-dimensional heated plane jet in a crossflow, where the jet was confined in a channel. In this flow configuration, the jet injected from a narrow slot developed between two sidewalls of the channel, without any clearance between the jet and walls. They reported on the two-dimensionality of the flow field, especially at the center of the slot. Sherif and Pletcher [6] made an experimental investigation of a round heated jet in crossflow for different velocity ratios of 1, 2, 4 and 7. They analysed the jet wake thermal characteristics for different velocity ratios. They found the difference of flow behaviour for small velocity ratios ($R < 2$) and large velocity ratios ($R > 2$). They observed the existence of a double vortex structure in the flow field for both the velocity ratios, but weaker in strength in small velocity ratio. Based on their results, they suggested that the velocity ratio $R = 2$ should be a borderline between the high velocity and low velocity ratios. Nishiyama et al. [30] reported the characteristics of temperature fluctuations in a slightly heated two-dimensional jet issuing through a slot normally into a crossflow for different velocity ratios. They studied the effects of the velocity ratio on the mean and fluctuating temperature fields. They observed that the low velocity ratio jets behave like a wall jet and the high velocity ratio jets are lift-off jets with a recirculation region. Said et al. [34] performed numerical investigation of a round heated jet in crossflow using different turbulence models. They reported the distribution of velocity, temperature field and mass fraction of different constituents of the jet. They observed that the velocity field fully controls the dilution of temperature and concentration of the jet. They also showed a better performance of the Reynolds-stress transport model compared to two-equation models.

Haniu and Ramaprian [35,36] experimentally studied a turbulent plane jet injected from a narrow slot into the crossflow in a channel. They performed the experiments for three values of jet to crossflow velocity ratios $R = 6$, 9 and 10 both for isothermal and heated jets. There was a small clearance between the slot and the sidewalls in their experiments. They performed the measurements of mean and turbulent flow properties in the middle of the jet slot and observed that both the mean velocity and temperature fields maintain two-dimensionality. Their observations did not include the effects of sidewalls. They used a two-channel LDA and resistance thermometry to measure the instantaneous velocity and temperature fields. They could

not resolve the different vortical structures of the flow field. Kalita et al. [37] numerically investigated the flow configurations of Ramaprian and Haniu [35,36] using the standard k–ε model and by assuming a two-dimensional mean flow. They observed a poor agreement between their predictions and the experimental data.

Much of the computational works reported in the literature for the analysis of jet in crossflow are using relatively simple turbulence model such as the k–ε model [38]. In most cases, the predictions by these simple models result in poor agreement with the experimental results. The failure of the numerical predictions can be attributed to inaccurate predictions of the Reynolds-stress tensor by the simple eddy-viscosity models, which do not represent the highly anisotropic nature of the flow appropriately. Since the flow field of jet in crossflow is highly complex and anisotropic, Reynolds stress transport model (RSTM), i.e., solving transport equations for different components of Reynolds stresses, can produce better results than those produced by the other two equation models. Demuren [39] has observed that RSTM reproduce peak vorticity and CRVP strength very well and predict Reynolds stresses better than that predicted by the k–ε model. Moreover, this model is computationally much less expensive than either LES or DNS.

Only a few literatures report the use of RSTM for investigation of the flow field of jet in crossflow. Ince and Leschziner [40,41] used a high-Reynolds number RSTM with wall functions to study the flow field of single and multiple jets in a crossflow. Demuren [39] also reported predictions with a high-Re model using a multigrid method and obtained fairly good predictions of the mean flow field. Jansson and Davidson [42] applied near-wall corrections to the basic linear model and solved a low-Reynolds number RSTM to predict effusion cooling in a double-row discrete-hole configuration. They reported better predictions than that by a two-layer k–ε model. Hale et al. [18] used commercial flow solver FLUENT to study the surface heat transfer associated with a row of short-hole jets in a crossflow. They used Reynolds-stress transport model with non-equilibrium wall functions and a two-layer zonal approach and found a better performance by two-layer zonal method than that by RSTM. The investigation done by Hale et al. [18] was for the multiple round jets in a crossflow. However, no work on the study of plane jet in crossflow using Reynolds-stress transport model has been reported in the literature.

1.1. Present work

The flow configuration for the present computations corresponds to the experimental work of Ramaprian and Haniu [35,36], where two-dimensional measurements were made for a slightly heated turbulent rectangular jet discharged into a crossflow. In the present work, the numerical investigations were undertaken using two different turbulence models, namely, the standard k–ε model and Reynolds stress transport model (RSTM). The objective of the present investigation is to obtain a better understanding of the flow physics than that obtained experimentally by Ramaprian and Haniu [35,36]. This is achieved by investigating the three-dimensional mean flow field and resolving several issues related to the flow three-dimensionality. The formation of different types of vortices and their effects on the mean velocity and temperature fields are discussed. The computational results are compared with the measurements of Ramaprian and Haniu [35,36] wherever available. The predictions of some flow properties, which were absent in the experimental observations, are also reported in the present work. Section 2 describes the flow configuration, governing equations, turbulence model, and the numerical procedure. The predictions of the mean and turbulent quantities and their comparisons with the measurements have been reported in Section 3 followed by conclusions in Section 4.

2. Problem description

A schematic of the three-dimensional computational domain used in the present work is shown in Fig. 1. It includes the jet discharge slot, two sidewalls and the entire three-dimensional region where an interaction between the jet and crossflow takes place. A rectangular slot jet is used and the jet discharge width is D, which is used as the length scale throughout the work. The origin of the coordinate system used was located at the center of the jet slot. The jet channel depth was $5D$ and the flow domain extended from $10D$ upstream of the center of the jet slot to $40D$ downstream. In the vertical direction, the domain extended $30D$ above the channel bed. In the spanwise direction, the distance between the two vertical sidewalls was $18D$ and the jet slot length in the spanwise direction was $10D$. The jet discharge and the flow in the entire computational domain were assumed fully turbulent and thus independent of the value of Reynolds number. The discharged jet was at a slightly higher temperature than that of the crossflow with a temperature difference of 5.70 °C. The value of the exit buoyancy Richardson number ($R_{\mathrm{bj}} = \frac{\Delta\rho_{\mathrm{j}} g D}{\rho_{\mathrm{a}} V_{\mathrm{j}}}$) due to heating was quite low thus ensuring a negligible buoyancy effect with heat simply playing the role of a passive scalar. In this condition, passive scalar such as temperature is transported only by the forced convective flow. It is logical to use the momentum ratio ($= \frac{\rho_{\mathrm{j}} V_{\mathrm{j}}^2}{\rho_{\mathrm{a}} U_{\mathrm{a}}^2}$) in the formulation of investigation of heated jet in crossflow, but since both the jets and crossflow are of the same fluid (water), the change of density for a small temperature difference was negligible. Thus, the momentum ratio is equivalent to velocity ratio.

2.1. Governing equations

The three-dimensional steady-state Reynolds-averaged Navier–Stokes and energy equations form the governing

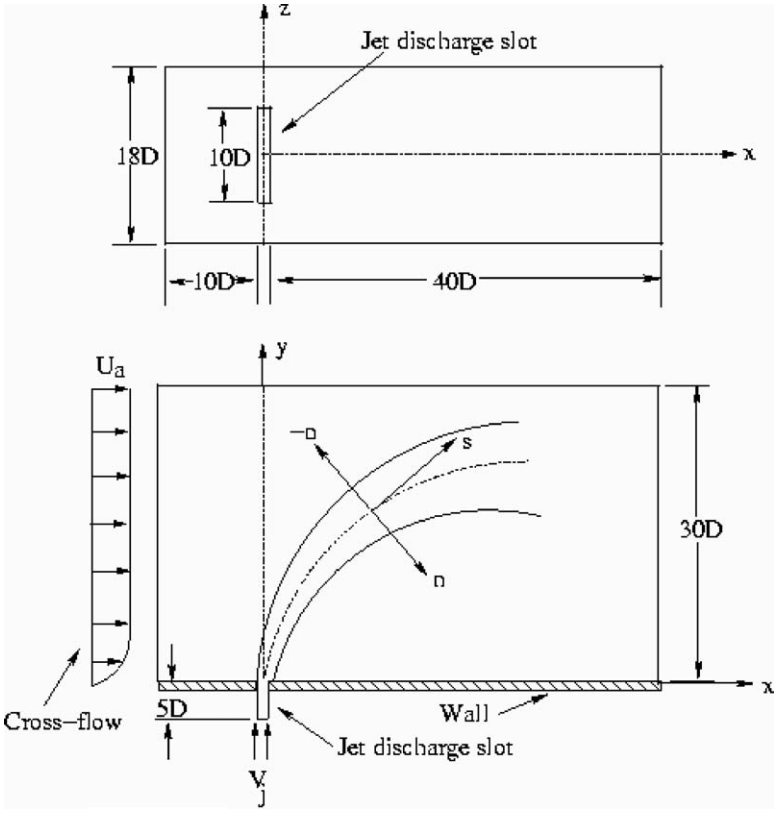

Fig. 1. Schematic diagram of the computational domain.

equations. The equations may be expressed in the conservative form using the Cartesian tensor notation as follows:

Continuity:

$$\frac{\partial}{\partial x_j}(\rho U_j) = 0, \tag{1}$$

Momentum:

$$\frac{\partial}{\partial x_j}(\rho U_i U_j) = -\frac{\partial P}{\partial x_i} + \frac{\partial}{\partial x_j}\left[\mu\left(\frac{\partial U_i}{\partial x_j} + \frac{\partial U_j}{\partial x_i}\right) - \rho\overline{u_i' u_j'}\right], \tag{2}$$

Energy equation:

$$\frac{\partial(\rho U_j T)}{\partial x_j} = \frac{\partial}{\partial x_j}\left[\left(\frac{\mu}{Pr} + \frac{\mu_t}{\sigma_t}\right)\frac{\partial T}{\partial x_j}\right]. \tag{3}$$

2.2. Turbulence model

The above-mentioned governing equations (1)–(3) require closure for the Reynolds stress tensor $\rho\overline{u_i' v_j'}$. The standard k–ε model and Reynolds stress transport model were used for the closure of the Reynolds stress tensor. In the standard k–ε model, the Reynolds stresses are modeled as

$$-\rho\overline{u_i' v_j'} = \mu_t\left(\frac{\partial U_i}{\partial x_j} + \frac{\partial U_j}{\partial x_i}\right) - \frac{2}{3}k\delta_{ij}, \tag{4}$$

where the eddy-viscosity is modeled as

$$\mu_t = \rho C_\mu \frac{k^2}{\varepsilon}. \tag{5}$$

For obtaining the k and ε terms, their individual transport equations were solved.

In RSTM, the closure is obtained by solving the time-averaged transport equations for the Reynolds stresses, which is given in the tensor notation as

$$\underbrace{\frac{\partial}{\partial x_k}(\rho U_k \overline{u_i' u_j'})}_{C_{ij}=\text{Convection}} = \underbrace{-\frac{\partial}{\partial x_k}[\rho\overline{u_i' u_j' u_k'} + \overline{p'(\delta_{kj}u_i' + \delta_{ik}u_j')}]}_{D_{ij}^{T}=\text{Turbulent diffusion}} + \underbrace{\frac{\partial}{\partial x_k}\left[\mu\frac{\partial}{\partial x_k}(\overline{u_i' u_j'})\right]}_{D_{ij}^{L}=\text{Molecular diffusion}} - \underbrace{\rho\left(\overline{u_i' u_k'}\frac{\partial U_j}{\partial x_k} + \overline{u_j' u_k'}\frac{\partial U_i}{\partial x_k}\right)}_{P_{ij}=\text{Stress production}} + \underbrace{\overline{p'\left(\frac{\partial u_i'}{\partial x_j} + \frac{\partial u_j'}{\partial x_i}\right)}}_{\phi_{ij}=\text{Pressure strain}} - \underbrace{2\mu\overline{\frac{\partial u_i'}{\partial x_k}\frac{\partial u_j'}{\partial x_k}}}_{\varepsilon_{ij}=\text{Dissipation}}. \tag{6}$$

To obtain the boundary conditions for the Reynolds stresses at the wall, the equation for the turbulent kinetic energy k was solved. Moreover the equation for the dissipation rate (ε) of turbulent kinetic energy was solved to obtain the dissipation rate (ε_{ij}) of Reynolds stress tensor. In both the equations a few minor modifications were made to the original form of the equations and they are as follows:

$$\frac{\partial}{\partial x_i}(\rho k U_i) = \frac{\partial}{\partial x_j}\left(\left(\mu + \frac{\mu_t}{\sigma_\varepsilon}\right)\frac{\partial k}{\partial x_j}\right) + \frac{1}{2}P_{ii} - \rho\varepsilon, \quad (7)$$

$$\frac{\partial}{\partial x_i}(\rho \varepsilon U_i) = \frac{\partial}{\partial x_j}\left(\left(\mu + \frac{\mu_t}{\sigma_\varepsilon}\right)\frac{\partial \varepsilon}{\partial x_j}\right) + \frac{1}{2}C_{\varepsilon 1}P_{ii}\frac{\varepsilon}{k} - C_{\varepsilon 2}\rho\frac{\varepsilon^2}{k}, \quad (8)$$

where P_{ii} is the production of turbulent kinetic energy and $\sigma_\varepsilon = 1.0$, $C_{\varepsilon 1} = 1.44$, $C_{\varepsilon 2} = 1.92$ are the model constants.

Among the various terms in Eq. (6), C_{ij}, D_{ij}^{L}, P_{ij} do not require any modeling. However, D_{ij}^{T}, ϕ_{ij}, and ε_{ij} need to be modeled to close the set of governing equations. The highly anisotropic nature of the flow due to streamline curvature near the jet discharge, resulting from a strong interaction between the jet discharge and crossflow, suggests that the production term and the pressure strain correlation play a dominant role in the prediction of turbulent stresses. The later process is especially important in producing the anisotropy of normal stress components. The quadratic pressure strain model proposed by Speziale et al. [43], which is known to improve the accuracy of flow field with streamline curvature, was used to model the pressure-strain term of the Reynolds-stress transport equation (Eq. (6)). Turbulent diffusive transport was modeled as suggested by Lien and Leschziner [44]. Dissipation term ($\varepsilon_{i,j}$) was modeled in terms of dissipation rate (ε) of turbulent kinetic energy as proposed by Sarkar and Balakrishnan [45]. It is to be noted that a Reynolds-stress transport model is applicable only for fully turbulent flows and not applicable in the vicinity of a solid wall, as it affects turbulent flow. In the near wall region, the molecular viscosity affects the generation, destruction and transport of the Reynolds stresses. Wall functions account for the shortcomings of the RST model in the near wall region. In the present work, the non-equilibrium wall functions that take care of the effects of strong non-equilibrium were used for resolving the near wall turbulence for both the models. The non-equilibrium wall functions employ the Launder and Spalding's log-law. However, the wall functions are also sensitized to the pressure-gradient effects, unlike the standard log-law. The employed non-equilibrium wall functions effectively relax the local equilibrium assumption of production equal to dissipation usually adopted in the standard wall function while computing the budget of the turbulence kinetic energy at the wall-neighboring cells. The values of Reynolds stresses were calculated from the adjacent wall cells by employing the wall functions. The Reynolds stresses at the wall adjacent cell were computed in terms of the turbulent kinetic energy k. See FLUENT 6.2 [46] for further details of the Reynolds-stress transport model used in the present work.

2.3. Numerical procedure

The numerical simulations were carried out using the commercial flow solver FLUENT 6.2.16 based on the finite volume method. The momentum and energy equations were discretized using the second-order upwind scheme and other transport equations were discretized using the power law scheme. The discretised equations were solved using the SIMPLE algorithm. Commercial package Gambit 2.1.6 was used to generate the geometry and mesh for the computational domain. Hexahedral elements were used for meshing the geometry. Different types of boundary conditions were used for different zones of the flow domain. For the crossflow and the jet discharge, the velocity inlet types of boundary conditions were used. At both the jet discharge and crossflow, the values of the mean and turbulent flow properties were prescribed according to the conditions in the experiments [35,36]. At the outlet of the computational domain (right boundary in Fig. 1), the outflow type of boundary condition was used. The no slip condition was used for the bottom wall, two sidewalls and the jet discharge channel walls. The upper boundary ($y/D = 30$) corresponds to a free surface with zero shear stresses. The temperature of the jet at the inlet was at 305.7 K and the temperature of the crossflow and all other wall temperatures were set at 300 K. In the computation, the mean velocity and temperature were normalized with the velocity and temperature of the jet, respectively. The implicit and segregated solver was used for the solution of the system of governing equations. All the variables were underrelaxed at each iteration. The solution was assumed to be converged when the normalized residual of the energy equation was lower than 10^{-6} and the normalized residuals of continuity and other variables were less than 10^{-3}. The computations were performed on a Pentium 4 machine with 256 MB RAM, 1.6 GHz processor speed and it took approximately 13 days of CPU time to achieve the converged solution. For studying the sensitivity of the computations to the grid resolutions, the flow field was obtained with three different grid resolutions (termed as the coarse, medium and fine grids). The numbers of cells in the three directions for the three grid resolutions are given in Table 1. The profiles of the turbulent kinetic energy at the jet center plane ($z/D = 0$) at the location of $x/D = 2$ using three different grid resolutions are shown in Fig. 2. The results corresponding to the coarse mesh show some deviation with respect to those obtained using other two resolutions (medium and fine). However, the predictions with medium and fine grid resolutions are close to each other. The results reported in the present paper correspond to that using the fine mesh. Note that a $4 \times 20 \times 40$ grid was used in the jet channel. The value of y^+ for the wall-adjacent cells was fixed approximately at 25. The grids at x–y and y–z planes are shown in Fig. 3.

3. Results and discussion

3.1. Mean flow field

The present predictions of the mean and turbulent flow properties were compared with the experimental data of Ramaprian and Haniu [35,36] for the value of jet to crossflow velocity ratio $R = 6$. It is to be noted that Ramaprian and Haniu [35,36] reported their experimental observations

Table 1
Number of cells for three different grid resolutions used

Mesh resolution	N_i (cells in x-direction)	N_j (cells in y-direction)	N_k (cells in z-direction)	N_{total}
Coarse	125	75	40	375,000
Medium	140	85	45	535,500
Fine	150	90	54	729,000

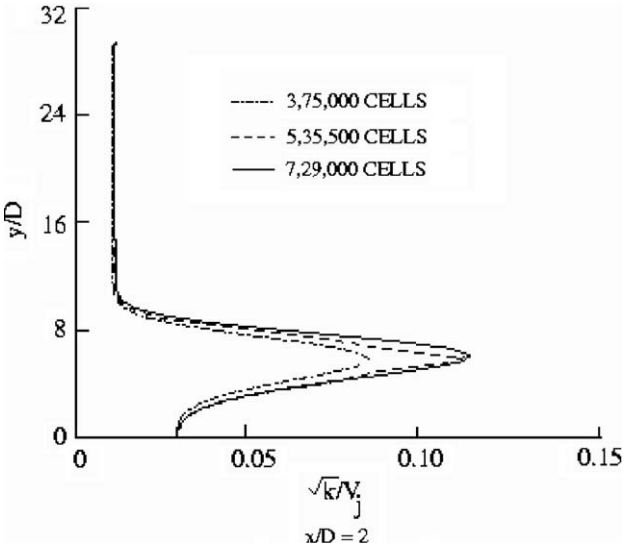

Fig. 2. Comparison of turbulent kinetic energy profiles at jet discharge center plane ($z/D = 0$) using different grid resolutions.

in the s–n co-ordinates, where s denotes the co-ordinate along the jet trajectory and n normal to the jet trajectory (Fig. 1). In the present work, the computations were performed in the Cartesian coordinates and the computed data was subsequently transformed to the s–n co-ordinates for the purpose of comparison with the experimental data. To gain an understanding of the flow physics in a clear way, first we have presented the predictions of the mean flow properties in the Cartesian coordinates.

The prediction of the mean streamwise velocity (U/V_j) at different downstream locations along the jet center plane ($z/D = 0$) are shown in Fig. 4. A reverse flow region is observed just downstream of the slot ($x/D = 2$). This reverse flow grows vertically and its strength increases further downstream ($x/D = 16$). The length of the recirculation region was found to be approximately 18 times the jet slot width. Further downstream ($x/D = 30$), the flow reattaches and recirculation region disappears. At $x/D = 2$, the difference in the predictions by the two models is small, whereas further downstream the predictions by the two models show deviations.

Fig. 5 shows the mean vertical velocity profiles (V/V_j) along the jet center plane ($z/D = 0$) at different downstream locations. Vertical velocities are stronger just downstream of the jet slot, as the jet is nearly vertical in this region. As the jet moves further downstream the vertical velocity reduces in magnitude and further downstream the jet becomes almost horizontal and the values of the vertical components are quite low. The standard k–ε model overpredicts compared to that by the RSTM.

The secondary motion in the vertical crossflow planes is presented by ploting the predictions of mean spanwise velocity profiles (W/V_j) in Figs. 6 and 7. The variations of the mean spanwise velocity at various downstream locations are shown at two different planes ($z/D = 3$ and -3). Let us first consider the flow at $z/D = 3$. At $x/D = 2$ the mean spanwise velocity near the lower surface is positive, which indicates that the flow is outward (towards sidewalls) and away from the jet center plane. Further downstream ($x/D = 10$ and 15) the velocities are negative close to the wall, indicating that the flow is towards the jet center plane. Just downstream of the jet slot, the jet pushes the crossflow towards the wall but further downstream the CRVP entrains the surrounding crossflow fluid towards the wall resulting in negative crossflow velocity near the wall. The velocity changes sign away from the wall representing the upper half of the CRVP, where the flow is moving away from the centerline. It is also observed that as the

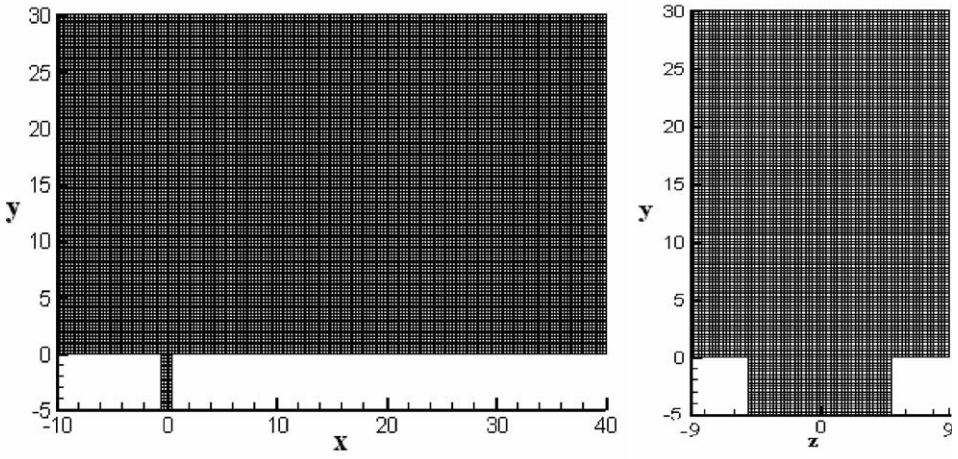

Fig. 3. Numerical grid at x–y and y–z plane (729,000 cells).

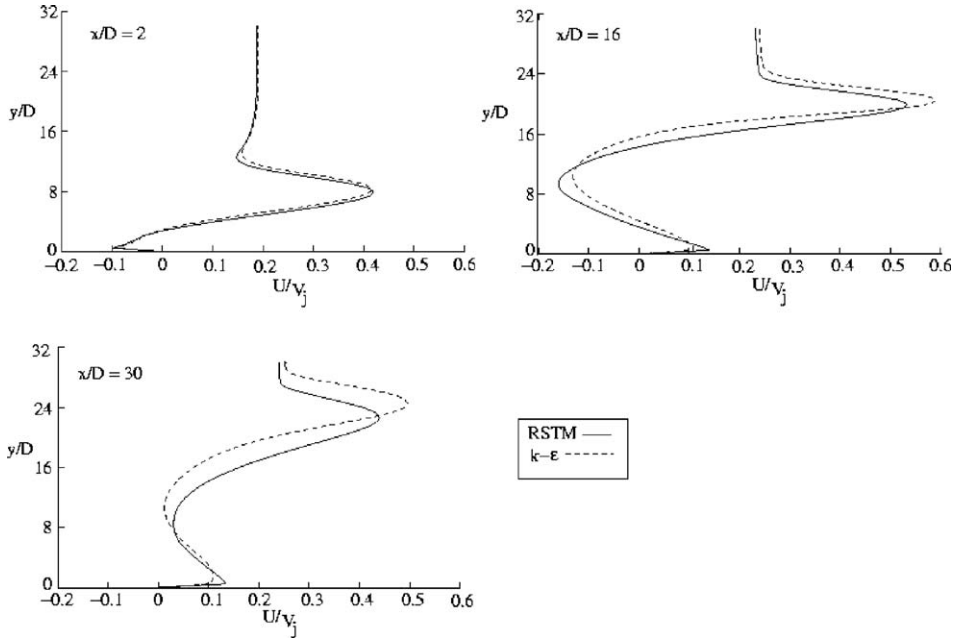

Fig. 4. Prediction of streamwise velocity at jet center plane ($z/D = 0$).

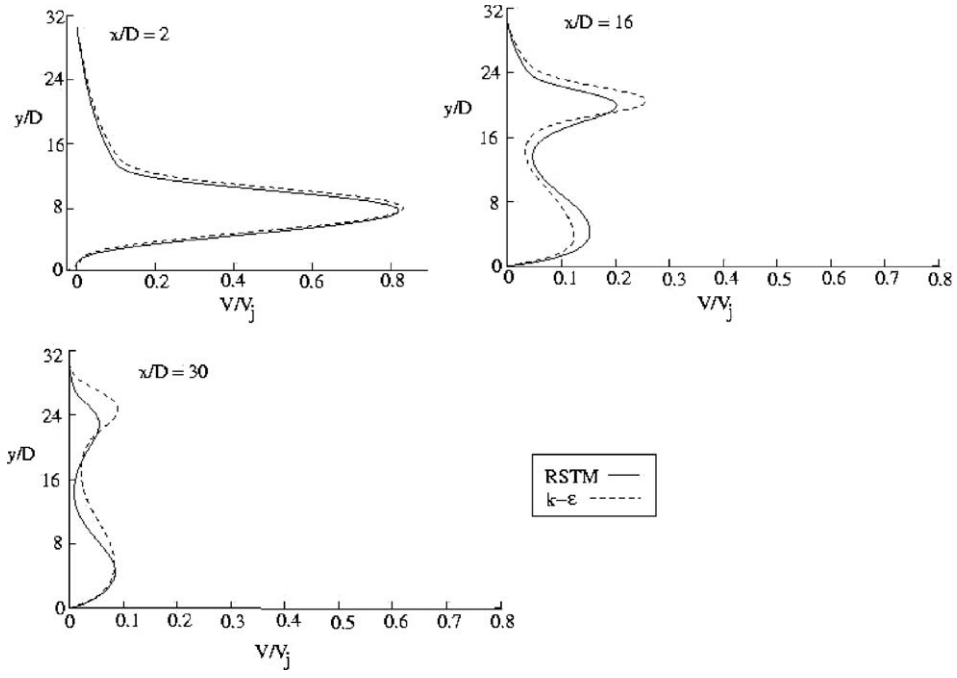

Fig. 5. Prediction of vertical velocity at jet center plane ($z/D = 0$).

flow progresses downstream the CRVP structures diminish in their strength. It is to be noted, that the trends of the mean velocity profiles (U/V_j, V/V_j and W/V_j) predicted in the present work resemble similar predictions for square jets in a crossflow [21–23]. At $z/D = -3$, W/V_j is opposite to that in $z/D = +3$ and from Figs. 6 and 7, it can be concluded that the flow is symmetric about the center plane, which is not true for the case of square jet in crossflow [22], that was slightly skewed in the lateral direction [22]. The flow field in the present flow configuration is symmetric due to the surrounding walls.

Variations of the mean spanwise velocity in the spanwise directions at a vertical distance of $y/D = 2$ from the channel bed and at two downstream locations are shown in Fig. 8. The spanwise velocity is symmetric about the center plane ($z/D = 0$). At a location just downstream of the jet discharge ($x/D = 2$), the velocity components show two different peak values in each half of vertical cross plane. It is

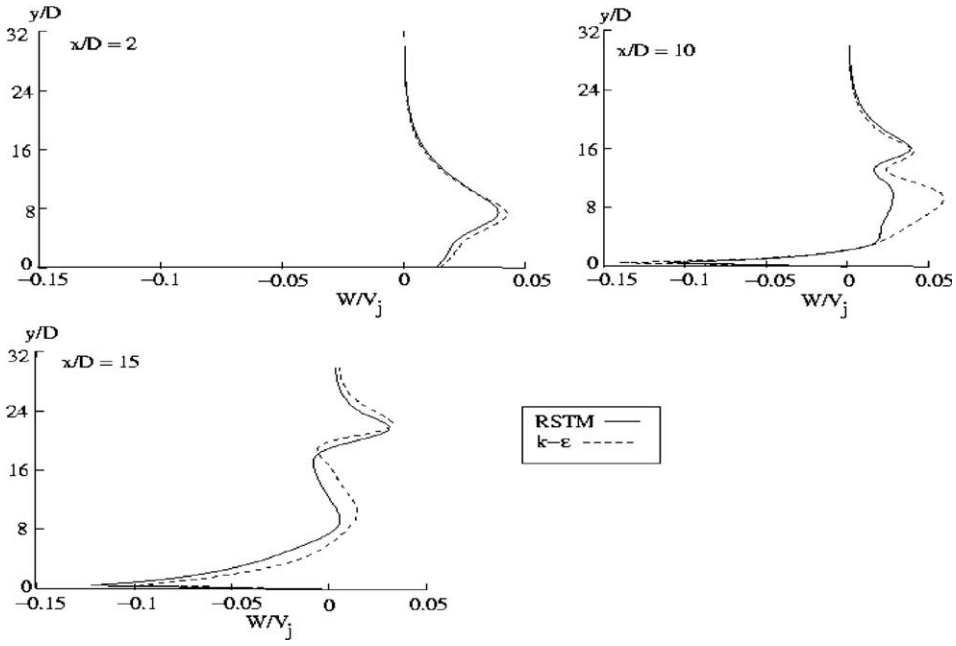

Fig. 6. Prediction of transverse velocity at the plane $z/D = 3$.

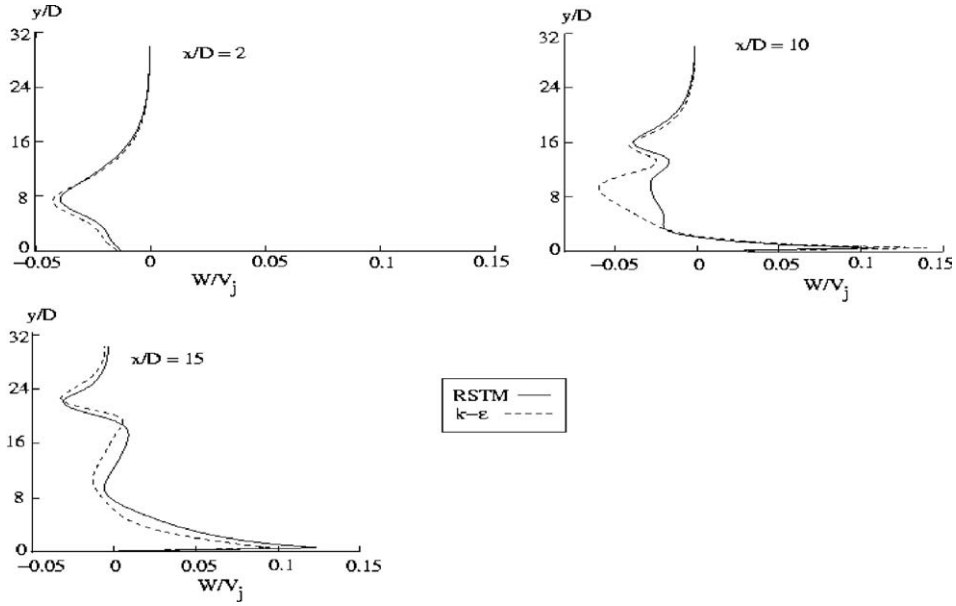

Fig. 7. Prediction of transverse velocity at the plane $z/D = -3$.

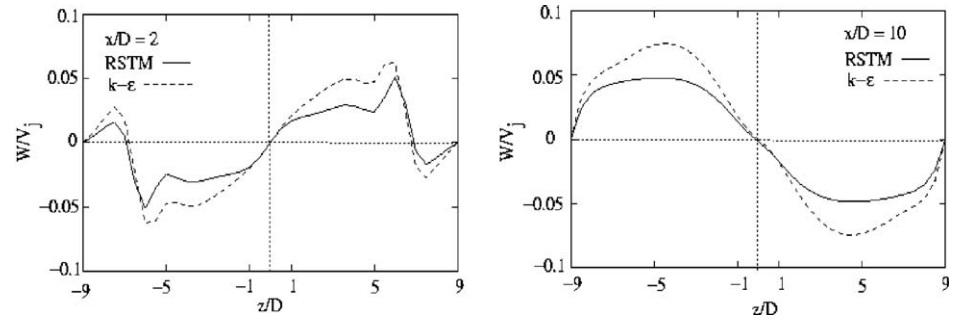

Fig. 8. Spanwise variation of transverse velocity at different x/D location.

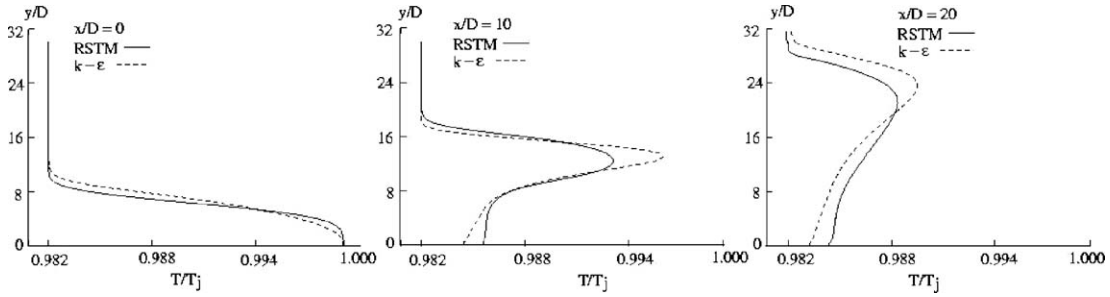

Fig. 9. Prediction of mean temperature at jet center plane ($z/D = 0$).

seen that CRVP form near the two sidewalls and their sizes are smaller than that of the two secondary vortices (Fig. 15). As the jet moves further downstream these two secondary vortices disappear and the CRVPs grow and dominate the flow field.

3.2. Mean temperature field

The normalized predicted mean temperature profiles (T/T_j) across the jet center plane at two different downstream locations are shown in Fig. 9. The distribution of the mean temperature at the upper and lower halves of the jet is different. This is due to the fact that distribution of the temperature in the lower half of the jet is controlled by recirculation. At the jet slot ($x/D = 0$), the peak of the mean temperature is near the wall, which indicates the high temperature of the jet stream at the jet inlet. Further, downstream the temperature peak moves upwards along with the jet and this spread is controlled by the CRVP. It is also observed that though the jet is slightly heated, the decay of the temperature with downstream distance is quite small, due to a weak crossflow.

3.3. Comparison with measurements

A comparison of the normalized s-component profiles of the mean velocity (U_s/V_j) across the jet center plane ($z/D = 0$) at two different downstream locations ($s/D =$ 4.94 and 13.88) with the experimental data is shown in Fig. 10. The overall agreement of the predictions by both the models is satisfactory and the performance of RSTM is better than that of the standard k–ε model. In the inner half of the jet, the standard k–ε model overpredicts the mean velocity thus predicting a small reverse flow region behind the jet.

Fig. 11 shows a comparison of the normalized n-component profiles of the mean velocity (V_n/V_j) across the jet center plane ($z/D = 0$) at two downstream locations ($s/D =$ 4.94 and 13.88) with the experimental data. The predictions agree well with the experimental data, both quantitatively and qualitatively. The RSTM model shows a higher level of recirculation, thus predicting a better recirculation compared to the standard k–ε model.

A comparison of the normalized temperature profile (T/T_j), across the jet center plane ($z/D = 0$) at two downstream locations ($s/D = 4.94$ and 13.88) with the experimental data is shown in Fig. 12. The recirculation and entrainment of the jet fluid results in a nearly uniform temperature distribution at the inner edge of the jet. Predictions of both the models agree well with the experimental data. However, the predictions by RSTM are superior to that by the standard k–ε model.

A comparison of the turbulent shear stress profiles across the jet is shown in Fig. 13. The large peak values observed in the experimental data and the present predictions are due to the high $\partial U/\partial y$ values in the jet-shear-layer region. The k–ε model overpredicts the shear stresses especially in the inner half of the jet, where the flow faces recirculation, whereas the RSTM agree well with the experimental results. Moreover, the predictions of the positive and negative peak values of the stresses by RSTM match well with the experimental data.

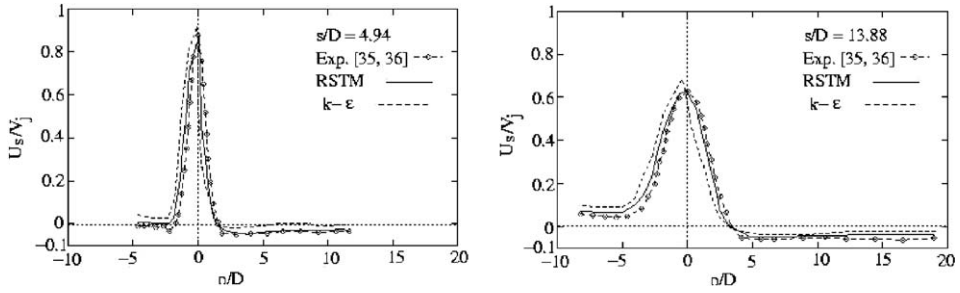

Fig. 10. Comparison of streamwise velocity at jet center plane ($z/D = 0$).

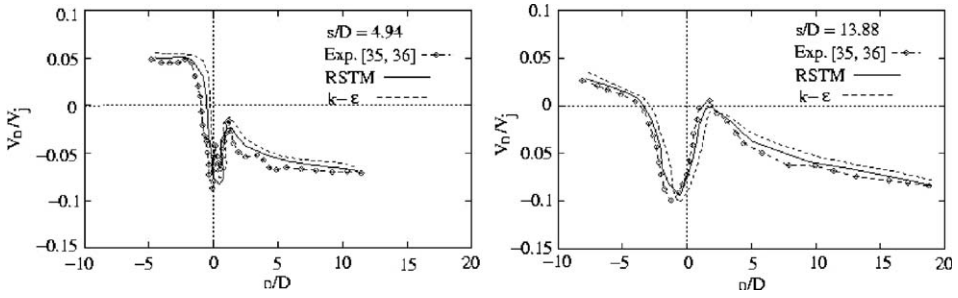

Fig. 11. Comparison of velocity at jet center plane ($z/D = 0$).

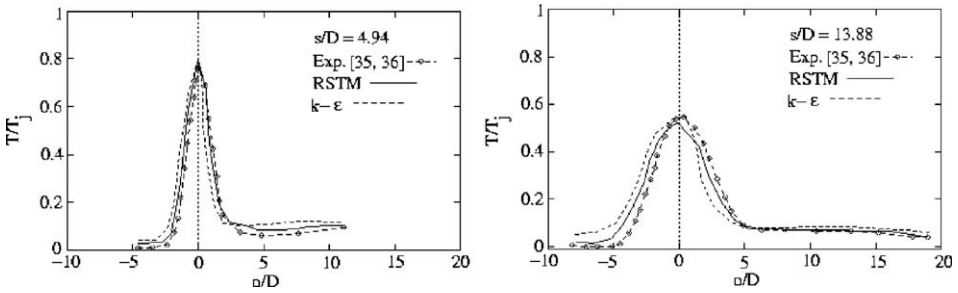

Fig. 12. Comparison of mean temperature at jet center plane ($z/D = 0$).

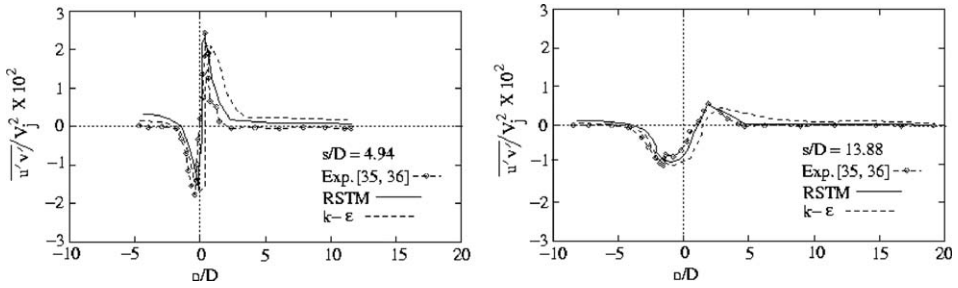

Fig. 13. Comparison of turbulent shear stress at jet center plane ($z/D = 0$).

3.4. Flow structures and their effects on the flow field

The predicted non-dimensional mean velocity vectors and streamline plot at three different x–y planes in the spanwise direction by the RSTM are shown in Fig. 14. The three planes chosen are the jet discharge center plane ($z/D = 0$) and planes at $z/D = 3$ and 5. The jet trajectory is deflected in the streamwise direction and the direction of the crossflow is altered as if a rigid obstacle blocks it. However, due to the jet entrainment effects and the motion of the jet, the flow field of jet in crossflow is different from that over a rigid obstacle. A reverse flow or recirculation is observed in the lower part of the jet, which indicates the existence of flow separation. The vertical penetration of the jet is more at the center plane ($z/D = 0$) than that at two other planes. This is due to the lateral spread of the jet near the edge of the jet discharge slot. It is also observed that the structures and extent of the recirculation regions downstream of the jet are different at the three planes, thereby demonstrating the three-dimensionality of the flow.

Fig. 15 shows the mean velocity field at different y–z planes at various x/D locations ($x/D = 0$, 2, 5 and 15). Upstream of the slot, the crossflow fluid starts to react to the upcoming jet disruption by moving upward. Due to the presence of jet, the crossflow experiences three-dimensional separation around the jet. The jet pushes the crossflow in the lateral direction at the edge of the discharge slot since the strength of the jet is more than that of the crossflow, but far downstream (at the plane $x/D = 15$) the trend is reversed.

The roll-up of the crossflow fluid into streamwise vortices at the edges of the jet is seen just downstream of the discharge slot ($x/D = 2$). At the center of the jet the inception of a pair of vortices is seen and another two vortical structures are present at both sides of jet slot edge. Further downstream of the jet slot ($x/D = 5$), the vortices produced at the slot edge have moved away from the channel bed and vortices formed at each side of the slot center plane increase in size. The direction of rotation of these vortices is opposite to that of the main vortices. These are the sec-

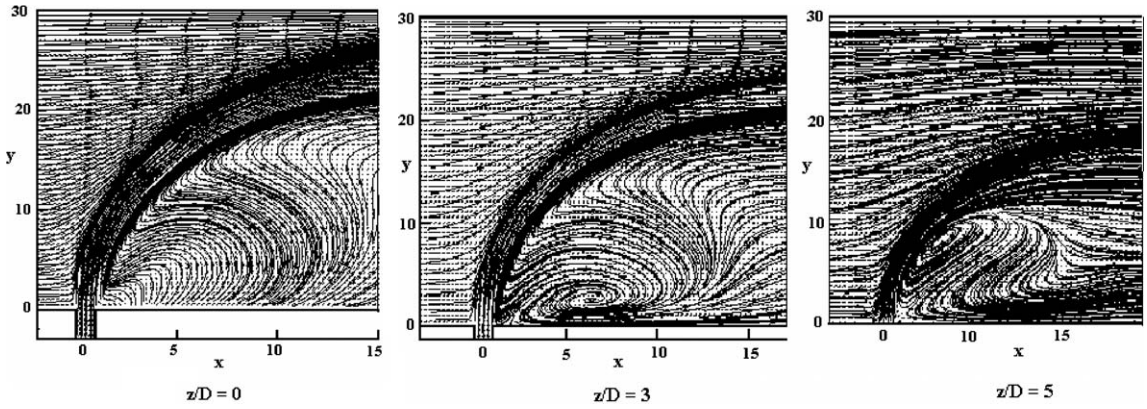

Fig. 14. Mean velocity vector and streamline plot at three spanwise x–y planes.

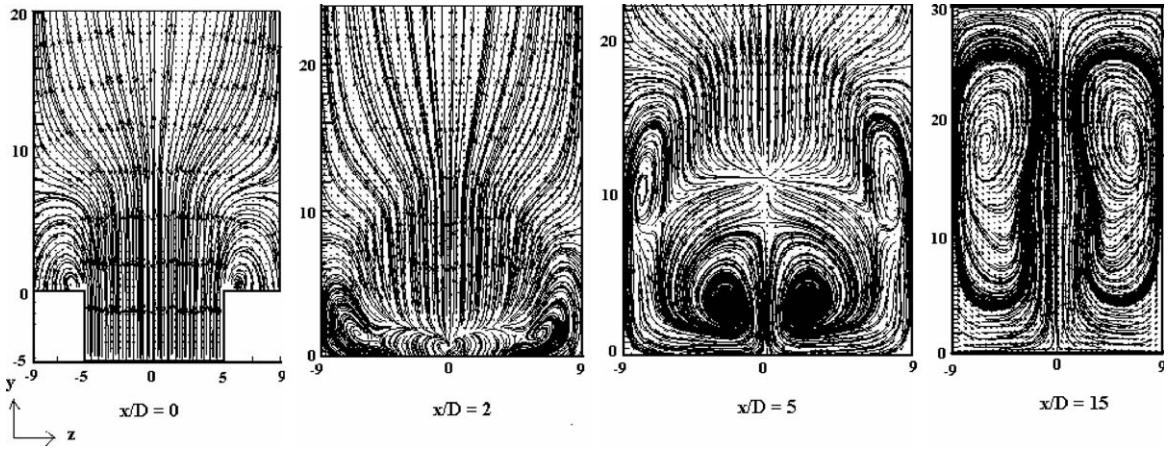

Fig. 15. Mean velocity vectors and streamline plot at different y–z planes in the direction of crossflow.

ondary vortices as reported by several researchers [9,15–18]. It is also observed that the secondary vortices reported here are more prominent in their size and strength compared to those reported in earlier studies [9,15–18]. The development of the CRVP becomes full fledged at $x/D = 15$, which grow in size and assume the shape of a kidney. The pressure drop in the wake region induces an inward motion, transporting the fluid from the crossflow towards the jet center plane.

Fig. 16 shows the mean velocity distributions of the jet stream into the crossflow at three different planes parallel to the channel bed. In the first plane ($y/D = 1$), the fluid at the streamwise centerline of the discharge slot is drawn outwards towards the edge of the jet. This is due to the entrainment process, where the jet and crossflow interact and exchange momentum. The crossflow is deflected due to the jet discharge. The crossflow is contracted between the sidewall and the edge of the jet slot and after crossing

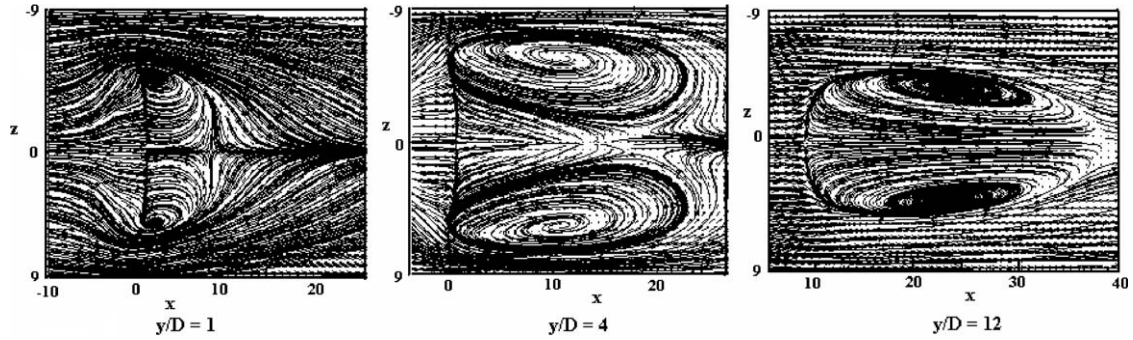

Fig. 16. Mean velocity vector and streamline plot in x–z plane at different y/D distance.

the slot the crossflow again expands and immediately downstream of the jet, two vortices roll-up. These vortices are stable wake vortices similar to that predicted by Hale et al. [18]. Downstream of these vortices fluid is still drawn strongly towards the jet centerline.

Continuing away from the channel bed to the plane at $y/D = 4$, the pair of vortices appear to have advected downstream and grown in size. Still further from the channel bed ($y/D = 12$), the contribution of the free-stream (crossflow) to the in-plane velocity magnitude increases owing to the bending of the jet. Therefore, velocity at this plane is larger in magnitude than that in the first two planes. As the jet bends and produces no blockage, the vortices diminish and disappear above this plane (not shown in Fig. 16). Iso-contours of the mean temperature at three different spanwise locations are presented in Fig. 17, which shows the shapes of well-known Gaussian distribution and the effect of the transport of the jet by the external crossflow. At the outer part of the jet, the distribution of the contour is dense, thus indicating that the mixing between the jet and the crossflow is rather active. In contrast, a quite coarse and relatively high temperature region is developed widely at the inner part of the jet. This originates from a low-velocity recirculating flow with large-scale eddies, which may promote the thermal spread process at the inner part of the jet. The spread of the mean temperature is affected by the mean velocity field at different spanwise locations. At the edge and outside of the slot, the spread of temperature is less compared to that at the center, which is similar to the case of the mean velocity field distribution.

Fig. 18 shows the mean temperature contours at various y–z planes at different downstream locations. In this case, also it is observed that the velocity field controls the distribution of the temperature field. The shape of the temperature distribution is more or less circular immediately downstream of the slot and it becomes kidney shaped further downstream. At all locations the shape is symmetric about $z/D = 0$ plane. It is observed that the CRVP dynamics controls the temperature distribution.

The mean temperature contours at various x–z planes at different heights are shown in Fig. 19, which shows that as the height (y/D) increases, temperature gets distributed over large region. Dispersion of the temperature is controlled by the pair of vortices, those formed in the x–z plane. The temperature distribution at different planes observed in the present work is similar to those reported in [30,34].

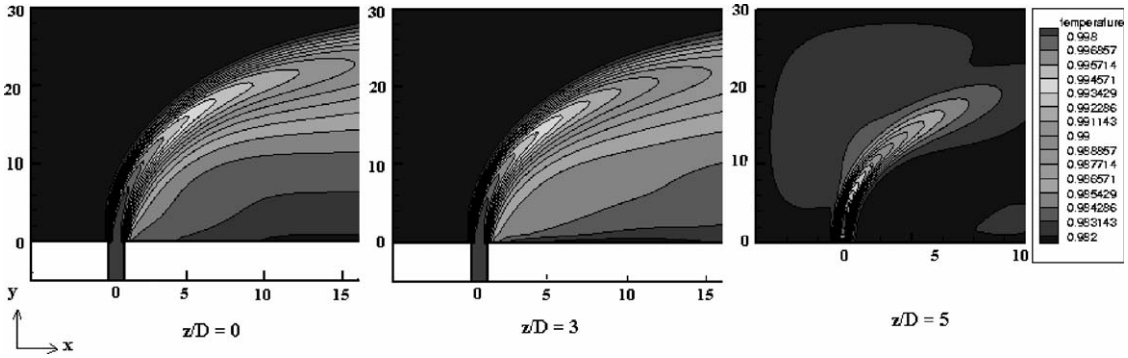

Fig. 17. Mean temperature contours at three spanwise x–y planes.

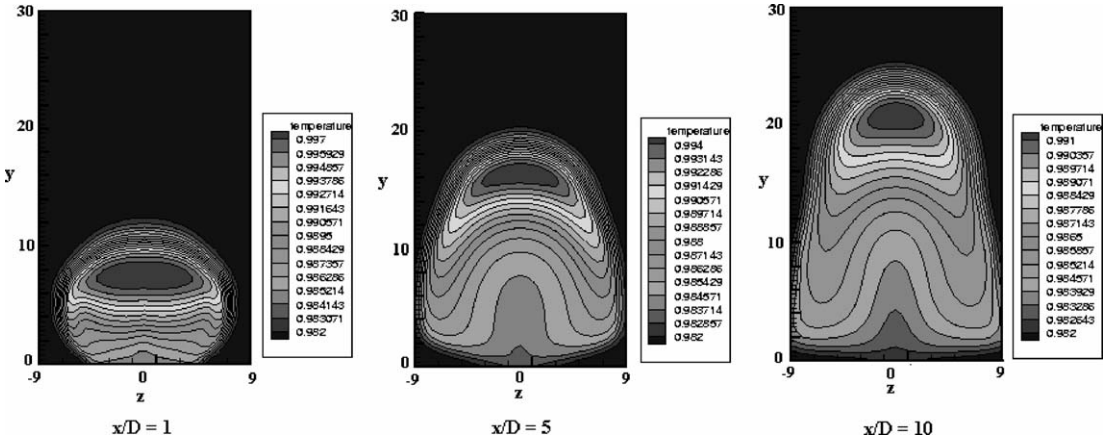

Fig. 18. Mean temperature contour at different y–z planes in the direction of crossflow.

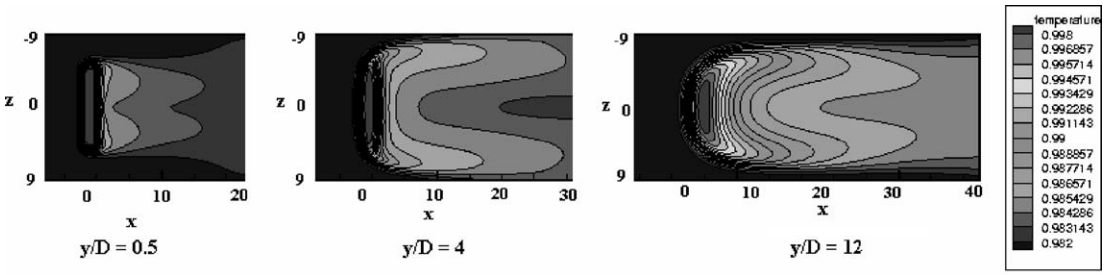

Fig. 19. Mean temperature contour in x–z plane at different y/D distance.

4. Conclusions

Three-dimensional mean flow field of a slightly heated jet discharged into a crossflow has been numerically investigated using the standard k–ε model and the Reynolds-stress transport model. The different terms of the Reynolds-stress transport model were modeled based on the proposals in the literature that are suitable for the present flow configuration. The predicted flow properties by both turbulence models were compared with the experimental data available in the literature. Some flow features that have not been reported in the literature were also predicted in the present work. The following conclusions may be drawn from the present investigation:

- Several issues of three-dimensionality of the flow field have been resolved in the present paper. It has been shown that the mean flow field exhibits complex interaction of the jet and crossflow resulting in flow expansion, contraction, and separation. The formations of different types of vortices were also shown in the flow field.
- Many physical phenomena, such as, entrainment, mixing are interrelated with different types of vortices observed in the present work. These vortices govern both the mean velocity and temperature fields.
- The overall mechanism of formation of different vortices and their structures in the present flow configuration are similar to the square jet in crossflow, though there is some qualitative difference in some vortices.
- The predicted mean flow properties such as velocity profiles, temperature profiles and turbulent shear stress by both the models are shown to be in good agreement with the experimental data. However, the Reynolds stress transport model is seen to perform better than the standard k–ε model.

References

[1] R.J. Margason, Fifty years of jet in cross-flow research, AGARD-CP 534, 1993.
[2] J.D. Holdeman, Mixing of multiple jets with a confined subsonic crossflow, Energy Combust. Sci. 19 (1993) 31–70.
[3] S.A. Sherif, R.H. Pletcher, The physical and thermal characteristics of the subsonic jet in a cross stream- a review, Mixed Convect. Environ. Flows 152 (1990) 83–94.
[4] S. Acharya, M. Tyagi, A. Hoda, Flow and heat transfer predictions for film cooling, heat transfer in gas turbine systems, Ann. NY Acad. Sci. 934 (2001) 110–125.
[5] A.O. Demuren, Modeling turbulent jets in cross flow, in: N.P. Cheremisinoff (Ed.), Encyclopedia of fluid mechanics, vol. 2, Gulf Publishing Company, Houston, TX, 1986 (Chapter 17).
[6] S.A. Sherif, R.H. Pletcher, Jet-wake thermal characteristics of heated turbulent jets in crossflow, J. Thermophys. 5 (1991) 181–191.
[7] N.M. Said, H. Mhiri, G.L. Palec, P. Bournot, Experimental and numerical analysis of pollutant dispersion from a chimney, Atmos. Environ. 39 (2005) 1727–1738.
[8] T.F. Fric, A. Roshko, Vortical structures in the wake of a transverse jet, J. Fluid Mech. 279 (1994) 1–47.
[9] R.M. Kelso, T.T. Lim, A.E. Perry, An experimental study of round jets in crossflow, J. Fluid Mech. 306 (1996) 111–144.
[10] J. Andreopoulos, W. Rodi, Experimental investigation of jets in a cross-flow, J. Fluid Mech. 138 (1984) 93–127.
[11] L.L. Yuan, R.L. Street, J.H. Ferziger, Large eddy simulations of a round jet in crossflow, J. Fluid Mech. 379 (1999) 71–104.
[12] A. Sau, T.W.H. Sheu, R.R. Hwang, W.C. Yang, Three-dimensional simulation of square jets in cross-flow, Phys. Rev. E 69 (2004) 066302-1–066302-20.
[13] T.T. Lim, R.M. Kelso, A.E. Perry, A study of a round jet in cross-flow at different velocity ratios, in: 11th Australian Fluid Mech. Conf., University of Tasmania, Hobart, Australia, 1992.
[14] S.D. Peterson, M.W. Plesniak, Short-hole jet in crossflow velocity field and its relationship to film cooling performance, Exp. Fluids 33 (2002) 889–898.
[15] S.D. Peterson, M.W. Plesniak, Evolution of jets emanating from short holes into crossflow, J. Fluid Mech. 503 (2004) 57–91.
[16] B.A. Haven, M. Kurosaka, Kidney and anti-kidney vortices in crossflow jets, J. Fluid Mech. 352 (1997) 27–64.
[17] D.M. Kuzo, An experimental study of the turbulent transverse jet, Ph.D. thesis, California Institute of Technology 1995.
[18] C.A. Hale, M.W. Plesniak, S. Ramadhyani, Structural features and surface heat transfer associated with a row of short-hole jets in cross-flow, Int. J. Heat Fluid Flow 21 (2000) 542–553.
[19] D.S. Liscinsky, B. True, J.D. Holdeman, Crossflow mixing of noncircular jets, J. Propul. Power 12 (1996) 225–230.
[20] M.J. Findlay, P. He, M. Salcudean, I.S. Gartshore, A row of streamwise inclined jets in crossflow: measurement and calculations, ASME-96-GT-167, 1996.
[21] P. Ajersch, S. Ketler, J.M. Zhou, I. Gartshore, M. Salcudean, Multiple jets in cross-flow: measurements and numerical simulations, ASME J. Turbomach. 119 (1997) 330–342.
[22] A. Hoda, S. Acharya, Predictions of a film coolant jet in crossflow with different turbulence models, ASME J. Turbomach. 122 (2000) 558–569.
[23] R. Keimasi, T. Rahni, Numerical simulation of jets in a crossflow using different turbulence models, AIAA J. 39 (2001) 2268–2277.
[24] R.P. Weston, F.C. Thames, Properties of aspect-ratio-4.0 rectangular jets in subsonic crossflow, J. Aircraft 16 (1979) 701–707.

[25] A.J. Humber, E.W. Grandmaison, A. Pollard, Mixing between a sharp-edged rectangular jet and transverse cross flow, Int. J. Heat Mass Transfer 36 (1993) 4307–4316.
[26] I. Vincenti, G. Guj, R. Camussi, E. Giulietti, PIV study for the analysis of planar jets in crossflow at low Reynolds number, in: ATTI 11th Convegno Nazionale AIVELA, Ancona, December 2–3, 2003.
[27] M.W. Plesniak, D.M. Cusano, Scalar mixing in a confined rectangular jet in crossflow, J. Fluid Mech. 524 (2005) 1–45.
[28] C.E. Wark, J.F. Foss, Thermal measurement for jets in disturbed and undisturbed crosswind conditions, AIAA J. 26 (1988) 901–902.
[29] K.S. Chen, J.Y. Hwang, Experimental study on the mixing of one and dual-line heated jets with a cold cross-flow in a confined channel, AIAA J. 29 (1991) 353–360.
[30] H. Nishiyama, T. Ota, M. Hamada, Y. Takahashi, Temperature fluctuations in a slightly heated slot jet issuing into a crossflow, Expt. Therm. Fluid Sci. 6 (1993) 252–262.
[31] S. Sarkar, T.K. Bose, Comparison of different turbulence models for prediction of slot-film cooling: flow and temperature field, Numer. Heat Transfer, Part B 28 (1995) 217–238.
[32] R.R. Hwang, T.P. Chiang, Numerical simulation vertical forced plume in a cross flow of stably stratified fluid, ASME J. Fluid Eng. 117 (1995) 696–705.
[33] Y. Shi, M.B. Ray, A.S. Mujumdar, Numerical study on the effect of cross-flow on turbulent flow and heat transfer characteristics under normal and oblique semi-confined impinging slots jets, Drying Technol. 21 (2003) 1923–1939.
[34] N.M. Said, H. Mhiri, S.E. Golli, G.L. Palec, P. Bournot, Three-dimensional numerical calculations of jet in an external cross flow: application to pollutant dispersion, ASME J. Heat Transfer 125 (2003) 510–522.
[35] H. Haniu, B.R. Ramaprian, Studies on two-dimensional curved non-buoyant jets in crossflow, ASME J. Fluids Eng. 111 (1989) 78–86.
[36] B.R. Ramaprian, H. Haniu, Turbulence measurements in plane jets and plumes in cross-flow, Technical Report No. 266, IIHR, University of Iowa, Iowa, 1983.
[37] K. Kalita, A. Dewan, A.K. Dass, Prediction of turbulent plane jet in crossflow, Numer. Heat Transfer, Part A 41 (2002) 1–12.
[38] S.V. Patankar, D.K. Basu, S.A. Alpay, Prediction of three-dimensional velocity field of a deflected turbulent jet, ASME J. Fluid Eng. 99 (1977) 758–762.
[39] A.O. Demuren, Characteristics of three-dimensional turbulent jets in crossflow, Int. J. Eng. Sci. 31 (1993) 899–913.
[40] N.Z. Ince, M.A. Leschziner, Calculation of single and multiple jets in crossflow with and without impingement using second-moment closure, in: Engineering Turbulence Modeling and Experiments, Elsevier, 1990, pp. 155–164.
[41] N.Z. Ince, M.A. Leschziner, Computation of three-dimensional jets in cross-flow with and without impingement using Reynolds-stress transport closure, in: AGARD Sym. Computational and Experimental Assessment of Jets in Crossflow, Paper 23, 1993.
[42] L.S. Jansson, L. Davidson, Numerical study of effusion cooling in a double-row discrete-hole configuration using a low-Reynolds stress transport model, in: Engineering Turbulence Modeling and Experiments, Elsevier, 1996, pp. 731–740.
[43] C.G. Speziale, S. Sarkar, T.B. Gataski, Modelling the pressure-strain correction of turbulence: an invariant dynamical systems approach, J. Fluid Mech. 227 (1991) 245–272.
[44] F.S. Lien, M.A. Leschziner, Assessment of turbulent transport models including non-linear RNG eddy-viscosity formulation and second moment closure, Comput. Fluids 23 (1994) 983–1004.
[45] S. Sarkar, L. Balakrishnan, Application of a Reynolds-stress transport model to the compressible shear layer, ICASE Report 90-18, NASA CR 182002, 1990.
[46] FLUENT 6.2, Users Guide, vol. 2, 2005, pp. 10.1–10.82.